Cavity-Enhanced Magnetooptical Observation of Magnetization Reversal in Individual Single-Domain Nanomagnets

ARTICLE *in* NANO LETTERS · AUGUST 2005

Impact Factor: 13.59 · DOI: 10.1021/nl050753p · Source: PubMed

8 AUTHORS, INCLUDING:

Naser Qureshi
Universidad Nacional Autónoma de México
21 PUBLICATIONS **44** CITATIONS
SEE PROFILE

James Alexander Liddle
National Institute of Standards and Technolo…
275 PUBLICATIONS **3,655** CITATIONS
SEE PROFILE

NANO LETTERS

2005
Vol. 5, No. 7
1413−1417

Cavity-Enhanced Magnetooptical Observation of Magnetization Reversal in Individual Single-Domain Nanomagnets

Naser Qureshi,[§] Suqin Wang, Mark A. Lowther,[†] Aaron R. Hawkins,[†] Sunghoon Kwon,[‡] Alexander Liddle,[‡] Jeffrey Bokor,[‡] and Holger Schmidt*

School of Engineering, University of California Santa Cruz, 1156 High Street, Santa Cruz, California 95064

Received April 22, 2005; Revised Manuscript Received June 10, 2005

ABSTRACT

Optical studies of nanoscale magnets promise access to ultrafast magnetization dynamics but are challenging because of limited spatial resolution. We demonstrate that cavity enhancement of the magnetooptical Kerr effect increases the sensitivity in nanomagnetooptics significantly. Magnetization switching in individual single-domain magnets in both far-field and near-field Kerr microscopy is observed, and scaling laws are determined. Near-field signals remain nearly constant with reduced magnet diameter, indicating favorable scaling of near-field magnetooptics into the deep nanometer range.

The use of patterned or self-assembled submicron ferromagnetic structures represents a promising approach to advances in high-density and high-speed magnetic information storage and has been investigated intensively in recent years.[1−9] At the 100-nm scale and below, nanomagnetic structures undergo a qualitative change and display single-domain behavior. By controlling the shape of the structure, the magnetization can be designed to point along one of two equilibrium directions, making nanomagnets attractive for patterned storage media. Magnetization rotation in these structures has been studied theoretically for many years.[10−14] In particular, it has been shown that the external magnetic field required to induce a reversal in the magnetization direction (switching field) depends on the interplay of nanomagnet shape and underlying crystal structure and that this important magnetic property can be tailored by designing the nanoparticle accordingly.[13,14] To study the underlying physics of the magnetization processes including switching fields and spin wave propagation, one needs to be able to observe individual nanomagnets and avoid ensemble averaging effects present in nanomagnetic arrays. Magnetic force microscopy (MFM) has been used successfully to determine switching fields of individual nanomagnets and reveal the influence of magnetostatic fields from neighboring particles in a high-density array.[4−7] However, MFM or giant magnetoresistance (GMR)[15,16] measurements can only provide static imaging of individual nanomagnets. To observe high-speed switching phenomena, we utilize optical techniques. Magnetization dynamics on the subnanosecond scale can be observed using the magnetooptic Kerr effect (MOKE),[1,7−9,17] and good spatial resolution has been achieved in some studies using high-NA immersion objective lenses.[17−22] However, to the best of our knowledge, no magnetooptic detection of switching in individual single-domain nanomagnets in the near or far field has been reported.

It is important to note that quantifying the ability to observe magnetization dynamics in an individual isolated nanomagnet requires a different figure of merit than that used when laterally scanning arrays of magnets to determine spatial resolution. In the case of a single magnet, the probe is stationary and the sensitivity to detecting a minute Kerr rotation signal from a nanometer-scale area are all important in resolving switching events. We have recently described a cavity-enhancement technique that leads to significantly increased MOKE signals by coating the magnetic surface with a dielectric material of the appropriate thickness for constructive interference in reflection.[23] The principle was demonstrated on nickel films, and it was pointed out that it should also be applicable to nanomagnetic structures. In this Letter, we report the use of cavity enhancement for enabling optical detection of magnetization reversal in individual

* Corresponding author. E-mail: hschmidt@soe.ucsc.edu.
† ECEn Department, Brigham Young University, 459 Clyde Building, Provo, UT 84602.
‡ Molecular Foundry, Lawrence Berkeley National Laboratory, Berkeley, CA 94720.
§ Present address: CCADET, UNAM, P.O. Box 70-186, 04511 Mexico D.F., Mexico.

10.1021/nl050753p CCC: $30.25
Published on Web 06/22/2005

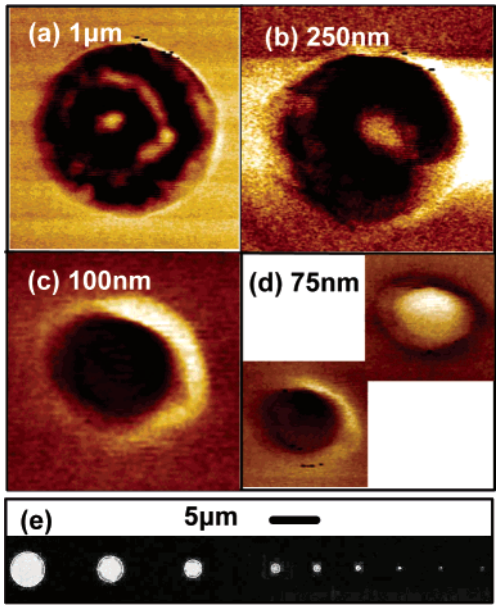

Figure 1. (a−d) MFM images of nickel magnets without an applied field single-domain behavior below 250 nm. (d) Two magnetization states of a 75-nm structure. (e) SEM images showing a sample layout (top view).

single-domain nanomagnets. We quantify the effect of cavity enhancement on the sensitivity of magnetooptic Kerr microscopy and show that it enables the far-field observation of structures with dimensions below 100 nm without the need for high numerical aperture immersion lenses. We also demonstrate that cavity enhancement enables near-field MOKE measurements of individual nanomagnets and that this near-field technique scales favorably with decreasing magnet dimensions. We introduce a geometric model that accurately describes the scaling of the MOKE signal with magnet dimension. These improved detection capabilities are a key enabler for future time-resolved magnetization studies of individual single-domain nanomagnets.

Here, we investigated nickel nanomagnets consisting of cylindrical pillars 150 nm in height with diameters ranging from 50 nm to 5 μm. They were fabricated by spinning a 350-nm-thick layer of KRS-XE resist[24] on a silicon substrate followed by patterning using electron beam lithography (Leica VB 6HR). Subsequently, the nickel pillars were formed with electron beam deposition and lift-off in dichloromethane with sonication.

The spacing between magnets was at least 5 μm to ensure that they were optically isolated in all of the measurements. MFM images taken at zero applied magnetic field show that structures 100 nm and smaller were magnetized out of the sample plane and contain only one domain. This domain shows only one of two magnetizations because of the shape anisotropy in the elongated pillars (Figure 1). The samples were coated with a 70-nm-thick silicon nitride layer using low-temperature plasma deposition (PECVD) to provide a Kerr enhancement of 5.0 as described previously.[23]

The experimental illumination setup common to all of the measurements described below is shown in Figure 2a. Individual magnets with diameter D are illuminated using

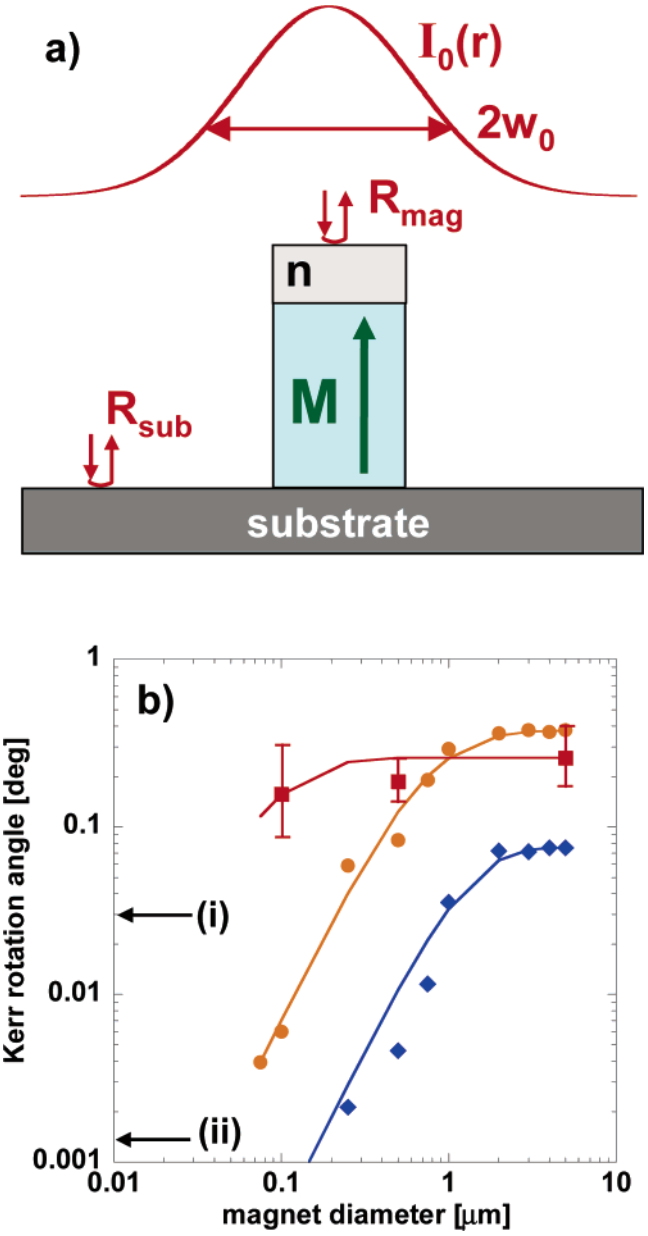

Figure 2. (a) Experimental setup: coated magnetic dots (reflectivity R_{on}) on substrate (reflectivity R_{off}) are excited with a Gaussian beam in the far field (spot size w_0). (b) Symbols: measured Kerr rotation ((◆): bare nickel magnets (far-field collection), (●): SiN-coated Ni dots (FF-collection), (■): SiN-coated dots (near-field collection, vertical bars: range of values measured), lines: fits to data using eq 3, arrows: noise levels, (i): near-field collection, (ii): far-field collection.

far-field optics. The spatial intensity distribution of the incoming beam ($I_0(r)$) is assumed to be Gaussian with a beam waist w_0. Generally, the beam is reflected partly by the magnetic material (reflectivity R_{mag}) and partly by the substrate (R_{sub}).

The effect of cavity enhancement on magnetooptic sensitivity was measured first using far-field MOKE detection. A beam from a 780-nm diode laser modulated at 1 kHz was focused onto the magnet of interest using a microscope objective (NA = 0.66). The linear polarization rotation of the reflected beam collected through the same objective was

measured using a photoelastic modulator (PEM), whose axis was perpendicular to the input polarization followed by a polarizer set at 45°, and a silicon photodiode. The polarization rotation angle θ (typically <0.1°) was determined from the reflected intensity at twice the PEM modulation frequency of 50 kHz and the signal at the laser modulation frequency, measured with two lock-in amplifiers:[25] $\theta = I(2\omega_{PEM})/[4J_2(\pi)I(\omega_{laser})]$. This corresponds to normalizing the Kerr-rotated signal by the total measured reflected intensity. A permanent magnet placed behind the substrate was rotated to reverse the sample magnetization, and the resulting change in polarization was recorded.

With uncoated nickel magnets, the smallest magnet with a discernible signal was 500 nm in diameter (Figure 2b, ◆). Without Kerr enhancement, the small size of single-domain magnets compared to the laser spot and the small magnitude of the intrinsic Kerr signal make the signal-to-noise ratio too low to observe single-domain magnets of 100 nm or less. When the same measurement was done with SiN-coated magnets, the Kerr rotation from larger structures was enhanced by a factor of 5 as expected given our results on unpatterned films.[23] We then detected magnetization reversal in structures that were four to five times smaller, including individual 100-nm and 75-nm single-domain magnets (Figure 2b, ●). To the best of our knowledge, these are the first far-field MOKE measurements on individual single-domain nanomagnets.

To quantify the experimentally observed scaling of the Kerr signal with the magnet dimensions, we developed a geometric model based on the illumination setup in Figure 2a. Only the fraction of light reflected from the magnet experiences Kerr rotation (α_0) and is modulated at $2\omega_{PEM}$ in the PEM. This intensity is given by

$$I_{R,\mathrm{mag}} = R_{\mathrm{mag}} \int_0^{D/2} 2\pi r I_0(r)\, \mathrm{d}r \tag{1}$$

The total signal used in the normalization process, however, also includes the part of the beam that was reflected from the substrate given by

$$I_{R,\mathrm{sub}} = R_{\mathrm{sub}} \int_{D/2}^{\infty} 2\pi r I_0(r)\, \mathrm{d}r \tag{2}$$

It is important to note that the reflected intensities depend on the respective reflection coefficients. The integration can be carried out analytically for a Gaussian beam with intensity $I_0(r) \propto e^{-2r^2/w_0^2}$, yielding the total size-dependent Kerr rotation angle α_{tot}.

$$\alpha_{\mathrm{tot}} = \alpha_0 \frac{I_{R,\mathrm{mag}}}{I_{R,\mathrm{mag}} + I_{R,\mathrm{sub}}} = \alpha_0 \frac{1}{1 + \frac{R_{\mathrm{sub}}}{R_{\mathrm{mag}}} \cdot \frac{1}{e^{D^2/2w_0^2} - 1}} \tag{3}$$

We fit the experimental data to eq 2 using experimentally determined reflection coefficients ($R_{mag} = 0.68$ and $R_{sub} = 0.35$ for bare nickel and $R_{mag} = 0.316$ and $R_{sub} = 0.046$ for SiN-coated magnets) and the Kerr angle observed on unpatterned films for α_0. The only free fitting parameter was the illumination beam spot size, w_0. The fits are added as solid lines in Figure 2b and show excellent agreement with the experiment for spot sizes of 1.35 (SiN coated) and 1.24 μm (bare Ni), respectively. The fact that the match between theory and experiment is excellent indicates that the magnet size does not noticeably affect the Kerr rotation (α_0) for dimensions of 75 nm or larger.

The improvement afforded by cavity-enhancement enabled detection of individual single-domain magnets with excellent sensitivity but without the need for a high-NA immersion lens. By using an immersion lens or a different coating,[23] we can detect magnetization changes in even smaller structures.

Next, we studied whether cavity-enhanced MOKE allows for the observation of single-domain nanomagnets in the near field. Being able to detect a magnetization signal with a near-field aperture on the order of 50−100 nm is important, especially for studying the effect of interactions from neighboring magnets in a high-density array. For typical spacings well below 100 nm, even a diffraction-limited spot from a high-NA lens would not be able to probe an individual nanomagnet. A near-field probe, however, will provide the required lateral resolution to collect MOKE from a single magnet and not its nearest neighbors. As mentioned above, this Letter focuses on demonstrating the necessary sensitivity of near-field MOKE microscopy rather than its lateral resolution for imaging. To this end, a commercial scanning probe microscope (DI Dimension 3100) was modified to hold and scan a tapered optical fiber tip. Materials and design were optimized to give very low levels of mechanical drift and to remain mechanically stable with large oscillating magnetic fields close to the sample. Here, the sample was illuminated through a lens, and reflected light was collected through a fiber tip. The polarization was analyzed using the PEM-based polarimeter described above and a photomultiplier tube (Figure 3). Aluminum-coated fiber probes were made with a meniscus etching method,[26,27] with apertures ranging from 0.1 to 1 μm and provided good polarization-maintaining characteristics with an extinction ratio better than 1:10.

The tip was brought close to the sample using a piezoelectric motion system, and an oscillation in collected light intensity was observed because of standing waves between the tip and sample. At subwavelength distances, the intensity decayed sharply (Figure 3a). This effect was used to monitor the tip−sample distance and maintain it in the near-field. Samples were scanned to produce a near-field optical image in intensity reflection mode, locate the magnet of interest, and estimate the effective tip aperture by observing its imaging resolution. The tip was then held stationary above a magnet. The extinction ratio of collected light was typically better than 1:10 after adjusting the bulk fiber curvature, and the polarization sensitivity of the probe in this position was verified by rotating the input polarization by a small known amount. A half-wave plate was then used to set the linear polarization at the PEM input to 90° to the PEM axis and define a zero polarization angle. An applied magnetic field

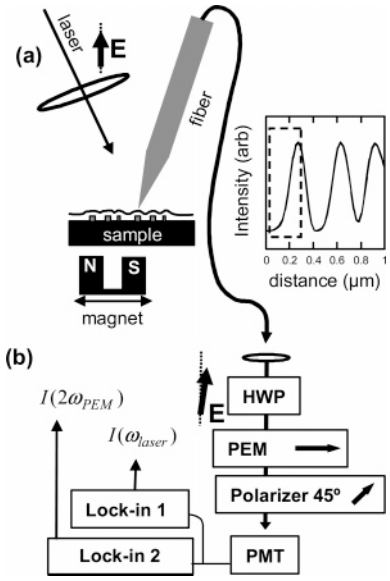

Figure 3. (a) Schematic of the near-field scanning probe system. Inset: light intensity collected through the fiber as a function of tip−sample distance. Dashed region indicates the near field. (b) Polarization analyzer based on photoelastic modulation at half-wave retardance.[25]

(<0.1 T) was reversed repeatedly every 20 s, and the local magnetization reversal events in the sample were detected. This time scale was found to give optimal signal-to-noise ratios, and drift in the apparatus ruled out longer measurement times. As a control, this procedure was repeated with the tip some lateral distance away from the magnetic structure to ensure that any polarization changes were due to the magnetooptic Kerr rotation and to rule out any spurious effects.

Magnetization reversal in SiN-coated magnets was measured in this way using a tip with subwavelength aperture size and tip−sample distance (Figure 2b, ■). As in the far-field case, the detected rotation for large dots (0.26°) was essentially identical to reference measurements on unpatterned nickel films (0.27°), indicating the reliability of the magnetooptic measurements. Repetitions of the measurement at different tip−sample distances (all below 0.8 μm) produced a range of polarization rotation angles (Figure 2b, vertical bars). The polarization extinction ratio exceeded 10:1 for each measurement. Although these variations are relatively large, they are not a problem for time-resolved measurements where time-dependent changes are monitored and the absolute value of the Kerr angle is of little importance. Magnetization reversals were clearly detected in individual 100-nm magnets (Figure 4). The most striking result is that the polarization signal stays, on average, nearly constant as the magnet size decreases, unlike the far-field signal that falls rapidly with reduced dimension. The weak signal dependence on magnet area is due to the fact that the near-field aperture is much smaller than the spot size and to first order; all of the detected intensity comes from the magnet and contributes to the Kerr signal. This indicates that the near-field technique outperforms far-field detection for studying single-domain nanomagnets and can be scaled down even further. The geometric model needs to be modified to

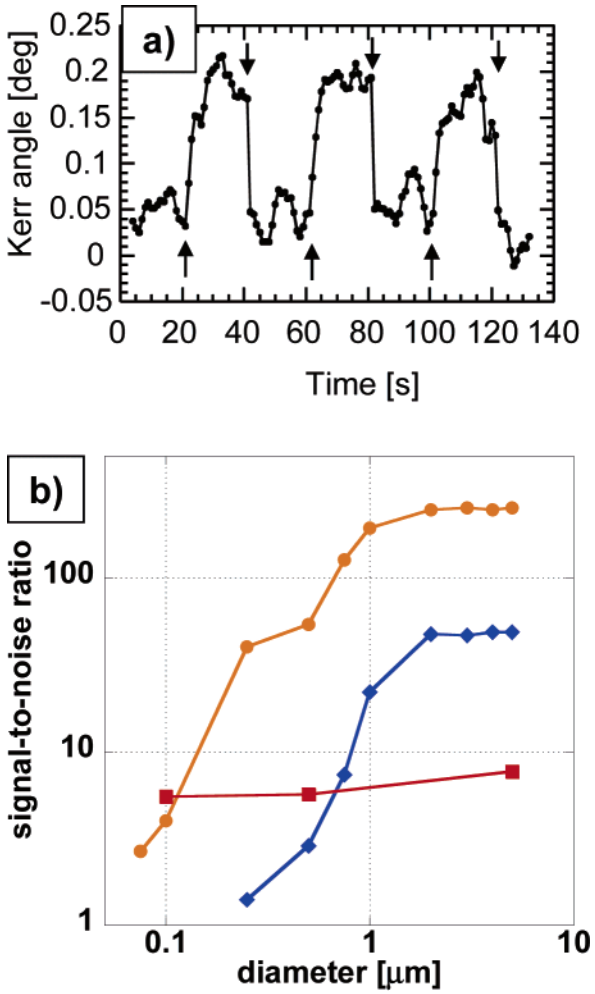

Figure 4. (a) Six magnetization reversal events (arrows) in a SiN-coated nickel magnet of 100-nm diameter measured in the near field. (b) Signal-to-noise ratio vs magnet diameter: bare nickel magnets, far-field detection (◆), SiN-coated magnets, far-field (●), SiN-coated magnets, near-field detection (■).

include the influence of the near-field aperture. In the first approximation, this can be done by assuming equal transmission across the aperture width and zero transmission for larger radii. This amounts to multiplying the reflected intensities with a Heaviside function $H(r - r_a)$ where r_a is the radius of the fiber tip and is given by

$$\alpha_{tot} = \alpha_0 \qquad \text{for } r_a < D \tag{4}$$

$$\alpha_{tot} = \alpha_0 \frac{1 - e^{-D^2/2w_0^2}}{1 - e^{-D^2/2w_0^2} + \frac{R_{sub}}{R_{mag}}(e^{-D^2/2w_0^2} - e^{-r_a^2/2w_0^2})} \qquad \text{for } r_a > D \tag{5}$$

Figure 2b shows a fit to the data using this approach. Again, good agreement with the experiment is found for an aperture diameter of 235 nm, very close to our expectations. The noise floor, taken to be the smallest MOKE distinguishable within an optimal 40-s period, was approximately 0.03° in the near-field compared to 0.0015° in the far-field measurement. Based on this, the mean signal-to-noise ratio

for the near-field measurement of a 100-nm magnet is 50% better than the far-field measurement. The dependence of the signal-to-noise ratio (SNR) as a function of magnetic dimensions is shown in Figure 4b. It can be seen that for large structures, far-field measurements have much better SNR and are clearly the preferred method. For single-domain nanomagnets, however, the SNR of the near-field technique exceeds that of the far-field measurement (50% in case of 100-nm magnets). The difference will be even bigger for smaller magnets.

We emphasize that the ability to carry out near-field reversal measurements is a direct result of the MOKE cavity enhancement because we were not able to distinguish clear Kerr signals from uncoated nickel magnets. Clearly, the SiN coating improves the polarization signal even when measured through a near-field probe. This shows that the cavity effect continues to work in an entirely near-field regime and provides the necessary signal-to-noise ratio at the 100-nm-length scale. Larger enhancements and hence further improved resolution and signal-to-noise ratios can be achieved with different coatings.[23] In addition, the SNR can be increased further by adding tip-height feedback in the setup.

In conclusion, we have demonstrated that cavity enhancement of the magnetooptic Kerr effect can be used to significantly increase the Kerr rotation measured from nanomagnetic structures and therefore the sensitivity of nanomagnetooptic measurements. We applied the technique to observe magnetization reversal in individual single-domain nanomagnets both in the near field and the far field. Sensitivity to sub-100-nm structures in the far field was achieved with a relatively inexpensive and low NA objective lens, but cavity enhancement in combination with high-NA immersion lenses can push the sensitivity in the far-field to smaller structures. Kerr enhancement remains effective when used on structures smaller than the wavelength of light, and the signal-to-noise ratio in near-field measurements scales favorably with magnet size, allowing for further reductions in size below 100 nm. Near-field MOKE will also provide the necessary spatial resolution to observe individual nanomagnets in close-packed arrays. We showed that the scaling of the Kerr signal with magnet dimension follows a geometric model. This allows for modeling and optimized design of the magnetooptical Kerr enhancement for a given magnetic structure. The improved sensitivity afforded by the cavity enhancement opens new possibilities for experiments on nanomagnets, including time-resolved studies of magnetization dynamics in individual single-domain magnets through a combination of ultrafast optics with NSOM.[28]

Acknowledgment. We thank A. Berger and J. Cerne for helpful discussions and B. Harteneck for experimental assistance with the nanomagnet deposition. This work was supported by the National Science Foundation under grants ECS-0245425 and ECS-0216155 and the Molecular Foundry at Lawrence Berkeley National Laboratory.

References

(1) Weller, D.; Sun, S.; Murray, C.; Folks, L.; Moser, A. *IEEE Trans. Magn.* **2001**, *37*, 2185.
(2) Chou, S. Y.; Wei, M.; Krauss, P. R.; Fischer, P. B. *J. Vac. Sci. Technol., B* **1994**, *12*, 3695.
(3) Sun, S.; Murray, C. B.; Weller, D.; Folks, L.; Moser, A. *Science* **2000**, *287*, 1989.
(4) Ross, C. A.; Hwang, M.; Shima, M.; Cheng, J. Y.; Farhoud, M.; Savas, T. A.; Smith, H. I.; Schwarzacher, W.; Ross, F. M.; Redjdal, M.; Humphrey, F. B. *Phys. Rev. B* **2002**, *65*, 144417.
(5) Abraham, M. C.; Schmidt, H.; Savas, T. A.; Smith, H. I.; Ross, C. A.; Ram, R. J. *J. Appl. Phys.* **2001**, *89*, 5667.
(6) Zhu, X.; Grutter, P.; Metlushko, V.; Illic, B. *J. Appl. Phys.* **2002**, *93*, 7059.
(7) Uhlig, W. C.; Li, H.; Han, B. S.; Shi, J. *J. Appl. Phys.* **2002**, *91*, 6943.
(8) Vavassori, P.; Zaluzec, N.; Metlushko, V.; Novosad, V.; Ilic, B.; Grimsditch, M. *Phys. Rev B* **2004**, *69*, 214404.
(9) Atkinson, D.; Cowburn, R. P. *Appl. Phys. Lett.* **2004**, *85*, 1386.
(10) Stoner, E. C.; Wohlfarth, E. P. *Philos. Trans. R. Soc. London, Ser. A* **1948**, *220*, 599.
(11) Brown, W. F., Jr. *Phys. Rev.* **1957**, *105*, 1479.
(12) Schmidt, H.; Ram, R. J. *J. Appl. Phys.* **2001**, *89*, 507.
(13) Aharoni, A. *J. Appl. Phys.* **1997**, *82*, 1281.
(14) Schmidt, H. *J. Appl. Phys.* **2003**, *93*, 2107.
(15) Schumacher, H. W.; Chappert, C.; Crozat, P.; Sousa, R. C.; Freitas, P. P.; Miltat, J.; Fassbender, J.; Hillebrands, B. *Phys. Rev. Lett.* **2003**, *90*, 017201.
(16) Kaka, S.; Russek, S. E. *Appl. Phys. Lett.* **2002**, *80*, 2958−2960.
(17) Choi, B. C.; Belov, M.; Heibert, W. K.; Ballentine, G. E.; Freeman, M. R. *Phys. Rev. Lett.* **2001**, *86*, 728−731.
(18) Hicken, R. J.; Barman, A.; Kruglyak, V. V.; Ladak, S. *J. Phys. D* **2003**, *36*, 2183.
(19) Bayer, C.; Park, J. P.; Wang, H.; Yan, M.; Campbell, C. E.; Crowell, P. A. *Phys. Rev. B* **2004**, *69*, 134401.
(20) Fumagalli, P.; Rosenberger, A.; Eggers, G.; Munnemann, A.; Held, N.; Guntherodt, G. *Appl. Phys. Lett.* **1998**, *72*, 2803−2805.
(21) Meyer, G.; Crecelius, T.; Bauer, A.; Wenger, D.; Mauch, I.; Kaindl, G. *J. Microsc.* **2003**, *210*, 209.
(22) Durkan, C.; Schvets, I. V.; Lodder, J. C. *Appl. Phys. Lett.* **1997**, *70*, 1323−1325.
(23) Qureshi, N.; Schmidt, H.; Hawkins, A. R. *Appl. Phys. Lett.* **2004**, *85*, 431−433.
(24) Medeiros, D. R.; Aviram, A.; Guarnieri, C. R.; Huang, W.-S.; Kwong, R.; Magg, C. K.; Mahorowala, A. P.; Moreau, W. M.; Petrillo, K. E.; Angelopoulos, M. *IBM J. Res. Dev.* **2001**, *45*, 639.
(25) Eggers, G.; Rosenberger, A.; Held, N.; Munnemann, A.; Guntherodt, G.; Fumagalli, P. *Ultramicroscopy* **1998**, *71*, 249.
(26) Monobe, S.; Ohtsu, M. *J. Lightwave Technol.* **1996**, *14*, 2231.
(27) Hoffmann, P.; Dutoit, B.; Salathé, E. *Ultramicroscopy* **1995**, *61*, 165.
(28) Levy, J.; Nikitin, V.; Kikkawa, J. M.; Awschalom, D. D.; Samarth, N. *J. Appl. Phys.* **1996**, *79*, 6095−6100.

NL050753P